Formulation and Implementation of Density Functional Embedding Theory using Products of Basis Functions

Vladimir V. Rybkin*

Department of Chemistry, University of Zurich, Winterthurerstrasse 190, Zurich 8057, Switzerland

E-mail: vladimir.rybkin@chem.uzh.ch

Phone: +41 44 63 54480

Abstract

The representation of embedding potential in using products of AO basis functions has been developed in the context of density functional embedding theory (DFET). The formalism allows to treat pseudopotential and all-electron calculations on the same footing and enables simple transfer of the embedding potential in the compact matrix form. In addition, a simple cost-reduction procedure for basis set and potential reduction has been proposed. The theory has been implemented for the condensed-phase and molecular systems using Gaussian and Plane Waves (GPW) and Gaussian and Augmented Plane Waves (GAPW) formalisms and tested for proton transfer reactions in the cluster and the condensed phase. The computational scaling of the embedding potential optimization is similar to this of hybrid DFT with a significantly reduced prefactor and allows for large-scale applications.

1 Introduction

Quantum-mechanical embedding is a multitude of methods for accurate and computationally feasible description of complex chemical environments.[1,2] Embedding methods are based on system partitioning in real or orbital space (or both), where subsystems interact with each other quantum mechanically. Embedding methods can be classified by the physical quantity transmitting the interaction:[3] local embedding potential,[4] matrix embedding potential,[5] density matrix,[6] Green's function[7] etc. There are, however, more variants of embedding theories not falling under this simple classification (*e. g.* embedded mean-filed theory[8] or bootstrap embedding[9]).

Subsystems are often described with different electronic structure methods. Some of them require accurate correlated wave function (CW) treatment, whereas the others as well as the interaction can be accurately described by density functional theory (DFT). This is particularly attractive for applications to extended systems with impurities, surface reactions on active sites, enzymatic reactions, reactions in solutions *etc.*, where correlated CW are necessary for accurate description, but not affordable due to the system size.

Thus, many embedding theories are multiscale methods and their implementation involves usage of several representations and often several software packages. The transformation between representations are often far from trivial, *e.g* transferring the embedding potential from periodic plane-wave DFT to the molecular CW solvers using Gaussian basis sets. In plane-wave DFT, the embedding potential is represented on a plane-wave grid and needs to be transformed to a one-electron term expressed in a Gaussian basis.[10,11] In periodic DFT implementations based on Gaussian functions, potentials are still expanded on an auxiliary plane-wave grid, so that the same problem persists. All-electron embedding calculations in this context are even more involved as different grids (both different from molecular grids) are used for the core and valence levels in the periodic DFT codes.[10]

In this work, we focus on developing an embedding potential representation in the context of unique-potential density functional embedding theory (DFET) to seamlessly link periodic

DFT using Gaussian basis functions with molecular wave function solvers. Although implemented and tested for DFET, the formulation can be applied to other embedding methods, based on embedding potentials, such as potential functional embedding theory (PFET)[12] and others.

2 Theory

2.1 Density functional embedding theory

In density functional embedding theory (DFET)[6] the energy of the total system partitioned into the cluster and the environment is generally given as:

$$E_{total}^{DFET} = E_{cluster}^{DFT}[\rho_{cluster}(\mathbf{r})] + E_{env}^{DFT}[\rho_{env}(\mathbf{r})] + E_{int}^{DFT}[\rho_{cluster}(\mathbf{r}), \rho_{env}(\mathbf{r})], \tag{1}$$

where the last term is the interaction energy between the subsystems. Within the unique embedding potential formalism,[6] the latter is defined as a functional derivative of the interaction energy with respect to both subsystem densities:

$$\frac{\delta E_{int}}{\delta \rho_{cluster}(\mathbf{r})} = \frac{\delta E_{int}}{\delta \rho_{env}(\mathbf{r})} = v_{emb}(\mathbf{r}) \tag{2}$$

Under unique embedding potential subsystem densities add up to give the density of the total system:

$$\rho_{total}(\mathbf{r}) = \rho_{cluster}(\mathbf{r}) \ - \rho_{env}(\mathbf{r}), \tag{3}$$

and embedded subsystems' energies are given as follows:

$$E_{cluster,emb}^{DFT} = E_{cluster}^{DFT}[\rho_{cluster}^{DFT}(\mathbf{r})] + \int v_{emb}(\mathbf{r})\rho_{cluster}^{DFT}(\mathbf{r})d\mathbf{r} \tag{4}$$

$$E_{env,emb}^{DFT} = E_{env}^{DFT}[\rho_{env}^{DFT}(\mathbf{r})] + \int v_{emb}(\mathbf{r})\rho_{cluster}^{DFT}(\mathbf{r})d\mathbf{r} \tag{5}$$

Embedding potential $v_{emb}(\mathbf{r})$ can be obtained by maximizing the Wu-Yang functional:[13]

$$W = E^{DFT}_{cluster,emb} + E^{DFT}_{env,emb} + \int v_{emb}(\mathbf{r})(\rho_{total}(\mathbf{r}) - \rho_{cluster}(\mathbf{r}) - \rho_{env}(\mathbf{r}))d\mathbf{r}, \tag{6}$$

where the embedding potential serves as a Lagrangian multiplier, and the functional derivative of W with respect to $v_{emb}(\mathbf{r})$ is simply a density difference:

$$\frac{\delta W}{\delta v_{emb}(\mathbf{r})} = \rho_{total}(\mathbf{r}) - \rho_{cluster}(\mathbf{r}) - \rho_{env}(\mathbf{r}). \tag{7}$$

As soon as embedding potential is obtained one can perform a correlated wave function (CW) calculation on the embedded cluster and compute the total energy in a linear approximation:

$$E^{DFET}_{total} = E^{DFT}_{total} + (E^{CW}_{cluster,emb} - E^{DFT}_{cluster,emb}) \tag{8}$$

This expression in the spirit of first-order perturbation theory is similar to the subtractive ONIOM scheme[14] is particularly simple, although other formulas have been proposed and tested.[6]

2.2 DFET with local basis sets

In the finite AO basis set $\{\phi\}$ electron density is given by:

$$\rho(\mathbf{r}) = \sum_{\mu\nu} P_{\mu\nu}\phi_\mu(\mathbf{r})\phi_\nu(\mathbf{r}), \tag{9}$$

where $P_{\mu\nu}$ is the density matrix in the AO basis.

One can expand the embedding potential in finite local basis $\{\phi\}$:[13]

$$v_{emb}(\mathbf{r}) = \sum_{\mu} v_\mu\phi_\mu(\mathbf{r}), \tag{10}$$

with the functional derivative:

$$\frac{dW}{dv_\mu} = \int (\rho_{total}(\mathbf{r}) - \rho_{cluster}(\mathbf{r}) - \rho_{env}(\mathbf{r}))\phi_\mu(\mathbf{r})d\mathbf{r} \to 0 \tag{11}$$

This formulation turns out to be inefficient[15] as the basis is not flexible enough to describe the potential concentrating in the interatomic regions.

It is possible to go further and expand embedding potential in the product space of AO basis functions:

$$v_{emb}(\mathbf{r}) = \sum_{\mu\nu} V_{\mu\nu}\phi_\mu(\mathbf{r})\phi_\nu(\mathbf{r}). \tag{12}$$

Then by combining equations 9 and 12 we obtain the Wu-Yang functional:

$$W[V_{emb}] = E_{cluster}[\rho_{cluster}] + E_{env}[\rho_{env}] + \sum_{\mu\nu\lambda\sigma} \Delta P_{\lambda\sigma} V_{\mu\nu} S^{\lambda\sigma}_{\mu\nu} = \tag{13}$$

$$E_{cluster}[\rho_{cluster}] + E_{env}[\rho_{env}] + \sum_{\lambda\sigma} \Delta P_{\lambda\sigma} \tilde{V}_{\lambda\sigma}, \tag{14}$$

where $S^{\lambda\sigma}_{\mu\nu}$ are four-center overlap integrals and

$$\tilde{V}_{\lambda\sigma} = \sum_{\mu\nu} V_{\mu\nu} S^{\lambda\sigma}_{\mu\nu}. \tag{15}$$

Its derivative is then given by:

$$\frac{dW}{dV_{\mu\nu}} = \sum_{\mu\nu\lambda\sigma} \Delta P_{\lambda\sigma} S^{\lambda\sigma}_{\mu\nu} = \Delta\tilde{P}_{\mu\nu} \to 0 \tag{16}$$

Equations 4 and 5 for a subsystem now take form:

$$E^{DFT}_{emb} = E^{DFT}[\rho^{DFT}] + \sum_{\lambda\sigma} P_{\lambda\sigma} \tilde{V}_{\lambda\sigma} \tag{17}$$

The evaluation the embedding term in this equation as well as in computing the Wu-Yang functional derivative (equation 16) is computationally analogous to the calculation of

the exchange contribution to the Fock matrix.

An alternative formulation using AO product basis set for embedding potential expansion has been proposed by Zhang and Carter.[16] The product basis suggested by Kollmar and Neese[17] is given by:

$$g_{\mu\nu}(\mathbf{r}) = \sum_{\lambda\sigma} S^{-1}_{\mu\nu,\lambda\sigma}\phi_\lambda(\mathbf{r})\phi_\sigma(\mathbf{r}), \tag{18}$$

where $S^{-1}_{\mu\nu,\lambda\sigma}$ are elements of the inverse of a flattened four-center overlap matrix . This choice of the basis simplifies the expressions for Wu-Yang functional derivative (equation 16), but implies a costly inversion of the four-center overlap. The potential then obtained using the density response function is very accurate, although the overall scaling of the procedure is $\mathcal{O}(N^6)$.[16] In addition, this representation does not in general preserve sparsity and locality, amenable for efficient computational algorithms.

2.3 Basis set and potential reduction

Up to this point it has been assumed that all subsystems share the same basis set. In practice, this means that the subsystems have to be appended with the rest of atoms present in the total system as ghosts. Consequently, the computational cost reduction of the correlated wave function calculation on the embedded cluster comes only from the reduction of the number of electrons, whereas the number of AOs and thus total number of MOs remain the same as in the full system.

Zhang and Carter proposed the quantum-information inspired Schmidt decomposition technique to reduce the number of orbitals to be used in the CW solver.[18] Here, we propose a pragmatic approach to the basis set and potential reduction based on the Mulliken charge analysis,[19] which allows to continue working with quantities in the local AO basis.

Mulliken charge analysis is performed on the density matrix, $\mathbf{P}$, and is known to suffer from basis set dependence. This is, however, the amenable property for finding basis function contributions to the embedding potential, $\tilde{\mathbf{V}}$.

In the spirit of Mulliken population analysis, the gross atomic contribution of atom A, GOC_A to $\tilde{\mathbf{V}}$ is computed as follows:

$$GOC_A = \sum_{\nu \in A} \sum_{\mu} |\tilde{V}_{\mu\nu}| \tag{19}$$

If the value of $GOC_A / \sum_M GOC_M < \epsilon$, where ϵ is a small number atom A with the corresponding basis functions should be removed from the system, unless it belongs to the embedded subsystem. If the contribution is larger than ϵ, the atom is present in the embedded subsystem as a ghost (*i.e.* only its basis functions). The embedding potential reduced to a smaller basis set is then obtained by projection:

$$\tilde{\mathbf{V}}' = \mathbf{P}\tilde{\mathbf{V}}\mathbf{P}^T, \tag{20}$$

where $\mathbf{P}$ is a rectangular projector matrix of $reduced\_basis\_size \times original\_basis\_size$. $P_{ij} = 1$ where i corresponds to the index of the basis function in the reduced basis set, and j to the index of the same function in the original basis set; other elements are zero.

The final energy is evaluated as follows:

$$E^{DFET}_{total} = E^{DFT}_{total} + (E^{CW}_{cluster,emb} - E^{DFT}_{cluster,emb})_{red}, \tag{21}$$

where the terms in parenthesis are evaluated in the reduced basis with the reduced embedding potential.

3 Implementation

DFET with the embedding potential expansion in AO product basis has been implemented in a developer version of the CP2K program meant for periodic and molecular calculations using the mixed Gaussian and plane waves basis approach.[20,21]

3.1 Workflow

General workflow of the current DFET implementation is shown in Figure 1. Since DFET is a top-down approach based on the reference density reconstruction, the algorithms starts with the DFT calculation on the total system to obtain $\rho^{total}(\mathbf{r})$ serving as a reference. After that, one iterates until condition 3 is fulfilled, *i. e.* the Wu-Yang functional (eq. 13) is maximized. The iteration consists of subsystem DFT calculations with embedding potential (eq. 17), checking the convergence and updating embedding potential $\mathbf{V}_{emb}$ (and, accordingly, one-electron embedding term $\tilde{\mathbf{V}}_{emb}$ eq. 15). Update $\mathbf{V}_{emb}$ is a gradient optimization (maximization) step, involving the evaluation of the Wu-Yang functional derivative (eq. 16). Since the subsystems share the basis, $\tilde{\mathbf{V}}_{emb}$ is computed once for both cluster and environment. Thus, the expensive exchange-like build is performed only twice per optimization steps: $\tilde{\mathbf{V}}_{emb}$ in eq. 17 and the derivative $\tilde{P}_{\mu\nu}$ in eq. 16.

3.2 Gaussian and (augmented) plane waves methods.

Gaussian and plane waves (GPW) method[22] allows for efficient periodic DFT implementation using Gaussian functions as a primary basis, used for representation of density and KS matrices. In addition, the auxiliary plane waves basis is employed, and the auxiliary density on the regular grid is introduced:

$$\tilde{\rho}(\mathbf{r}) = \frac{1}{\Omega} \sum_{\mathbf{G}} \tilde{n}(\mathbf{G}) \exp(i\mathbf{G} \cdot \mathbf{r}), \tag{22}$$

where coefficients Ω is the volume of the unit cell, $\mathbf{G}$ are lattice vectors, and coefficients $\tilde{n}(\mathbf{G})$ are selected so that $\tilde{\rho}(\mathbf{r})$ is equal to $\rho(\mathbf{r})$. Auxiliary density expanded in plane waves, $\tilde{\rho}(\mathbf{r})$, is used to evaluate integrals and KS matrix terms in a computationally efficient manner. Since regular grid is sparse, it can only describe soft densities and is applicable to calculations with pseudopotentials describing the core levels.

Its extension for all-electron calculations (applicable also to pseudopotential calculations)

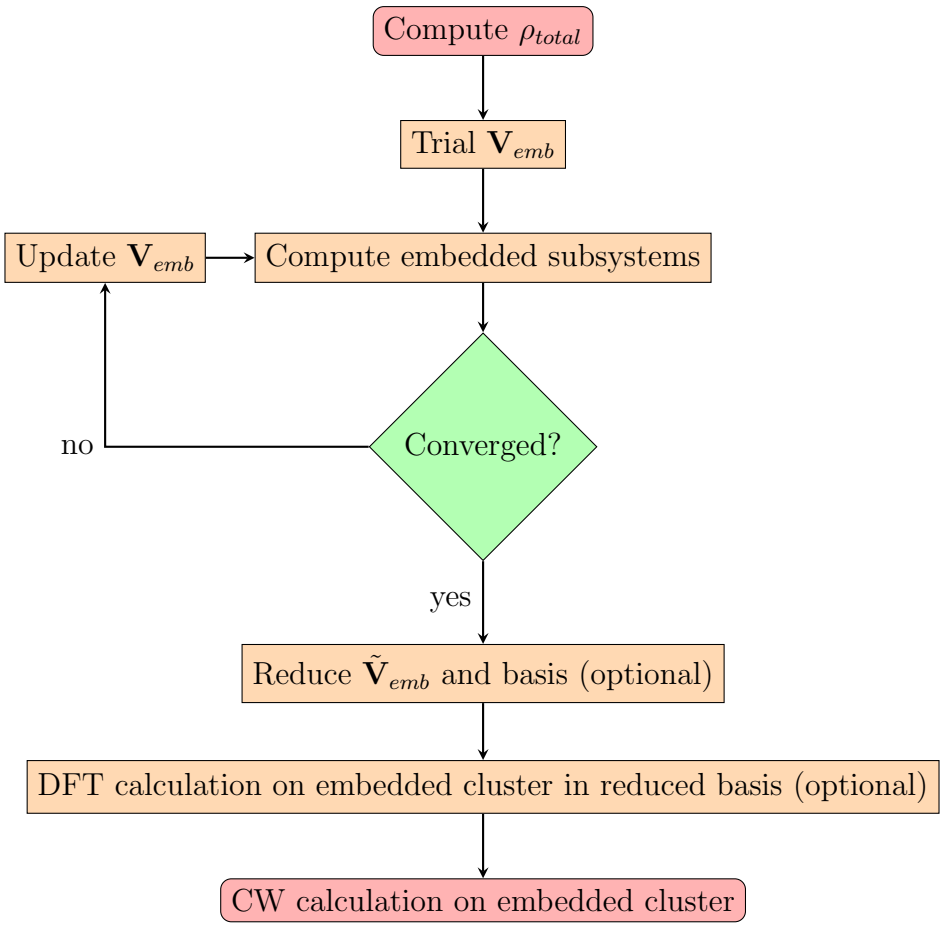

Figure 1: Workflow of DFET implementation using product basis expansion of the embedding potential.

is Gaussian and augmented plane waves (GAPW) method.[23] Within the GAPW approach, the auxiliary density is represented as a sum of three components:

$$\tilde{\rho}(\mathbf{r}) = \tilde{n}(\mathbf{r}) + \tilde{n}^1(\mathbf{r}) - n^1(\mathbf{r}), \tag{23}$$

where $\tilde{n}(\mathbf{r})$ is a soft density on the regular grid and the other two are atomic hard and soft densities, respectively:

$$n^1(\mathbf{r}) = \sum_A n^1_A(\mathbf{r}) \tag{24}$$

$$\tilde{n}^1(\mathbf{r}) = \sum_A \tilde{n}^1_A(\mathbf{r}) \tag{25}$$

Here summation runs over atoms A. The hard atomic density $n^1(\mathbf{r})$ is used for core levels and is expanded on a dense radial grid.

Evaluation of the embedding contribution to the KS matrix if the potential is expanded on the grid $v_{emb}(\mathbf{r})$ is straightforward in case of GPW or any other pseudopotential formalism using a uniform grid. For all-electron calculations with GAPW (or any multi-grid equivalent) one has to either employ a three-fold representation similar to the one of the density with the necessity to compute the cross terms in $\int v_{emb}(\mathbf{r})\tilde{\rho}(\mathbf{r})d\mathbf{r}$. Alternatively, one can keep the embedding potential on the regular grid and transform it to the dense radial grid to evaluate the hard density contribution, which is not trivial. In addition, this leads to modification of the Wu-Yang functional and its derivative. The corresponding formalism has been derived and implemented in the context of plane-wave DFT[10] within all-electron projector-augmented plane waves (PAW) formalism.[24]

Using matrix representation of embedding potential allows to circumvent the problem of density and potential representation and treat pseudopotential and all-electron cases (here, GPW and GAPW formalisms) on the equal footing, provided that the four-center overlap integrals are available.

3.3 Four-center overlap integral evaluation.

The key component of the current DFET implementation is the evaluation of four-center overlap integrals $S_{\mu\nu}^{\lambda\sigma}$ necessary for computing both Wu-Yang functional derivative (eq. 16) and one-electron embedding term (eq. 15). Despite the fact that that DFT calculations use GPW and GAPW methods for integral evaluation, four-center overlaps in the embedding part employ analytical Obara-Saika technique[25] as implemented in the libint library,[26] using the same CP2K machinery as for the exact exchange integral evaluation.[27] This trick allows avoiding tedious and potentially inefficient implementation of $S_{\mu\nu}^{\lambda\sigma}$ within GPW and GAPW formalisms of little relevance outside of embedding context. Moreover, embedding based on analytically computed $S_{\mu\nu}^{\lambda\sigma}$ are seamlessly applicable to both all-electron (GAPW) and pseudopotential calcualtions (GPW, also possible with GAPW). Indeed the embedding contribution is provided as a matrix and can be added to the KS matrix, independently of how each term was computed. This will be consistent if integration accuracies within DFT and embedding parts of the calculation are compatible, as demonstrated for hybrid functional DFT and coupled-perturbed updates for MP2 forces.

Four-center overlap integrals can also be evaluated employing the resolution-of-identity (RI), or density fitting approximation:[28]

$$S_{\mu\nu}^{\lambda\sigma} = (\mu\nu\lambda\sigma) = \sum_{PQ}(\mu\nu P)(PQ)^{-1}(Q\lambda\sigma) = \sum_{PQ} S_{\mu\nu}^{P} S_{PQ}^{-1} S_{\lambda\sigma}^{Q}, \tag{26}$$

where $S_{\mu\nu}^{P}$ and S_{PQ} are three- and two-center overlap integrals and $P, Q, ...$ denote auxiliary Gaussian basis functions, which are generated automatically.

Due to sparsity of overlap matrices $S_{\mu\nu}^{\lambda\sigma}$ can be computed efficiently using Schwarz screening, employing loose thresholds.[29] Moreover, similarly to the exchange integrals implemented in CP2K, it is possible to store $S_{\mu\nu}^{\lambda\sigma}$ in core with reduced requirements to memory, so that the integrals can only be computed once during the whole Wu-Yang functional maximization.

3.4 Tensor contractions

As the four-center overlap integrals can be computed only once, the two-index tensor contractions in computation of the Wung-Yang functional derivative (eq. 16) and one-electron embedding term (eq. 15) remain computational bottlenecks of the algorithm. Since both subsystems share the same basis, one only have to construct $\tilde{V}_{\mu\nu}$ once for both of them. The second contraction per iteration is needed to computed the gradient. Thus, only two two-index contractions are performed in one optimization step.

In CP2K, KS and density matrices are stored in a special sparse matrix format, taking advantage of sparse linear algebra based on the dbcsr library.[30,31] Thus, all matrix quantities relevant for DFET, $V_{\mu\nu}$, $\tilde{V}_{\mu\nu}$, $\Delta P_{\mu\nu}$ are also stored as sparse dbcsr matrices. This allows efficient two-index contractions "out of the box".

3.5 Optimization and acceleration convergence

Wu-Yang functional in matrix form (eq 13) is maximized using the conjugate-gradient method using Polak-Ribiere step update.[32] Our practice with grid-based DFET shows that using Fermi-Amaldi potential as initial guess leads to little if any acceleration of convergence as compared to a zero initial embedding potential. Therefore, in the current DFET implementation using AO product basis we start from a zero matrix potential, although we believe it is possible to construct physically motivated guess close to the converged embedding potential.

Since the workflow assumes repeated DFT calculations on the subsystems under changing embedding potential it makes sense to exploit density extrapolation from previous embedding iterations to construct initial orbital/density matrix guess. The always stable predictor corrector technique implemented in CP2K in context of molecular dynamics and geometry optimization provides accurate guess and faster SCF convergence also for DFET calculations.

4 Results and Discussion

Here we apply the presented formulation implementation of DFET to two systems: a toy one in the gas phase and a realistic liquid one. The first application is performed with pseudopotentials (GPW formalism), whereas the second with all electrons included (GAPW formalism). High-level methods selected to test the performance of the embedding, rather than to obtain the most accurate results. In this we have been restricted to the functionality of CP2K, where MP2[33] and RPA[34] are the most accurate available methods.[20]

4.1 Toy system: solvated proton transfer

As a proof-of-concept study we performed pontetinal energy scans for the proton transfer reaction in $(HFH^-)(H_2O)_4$ cluster shown in Figure 2(a). This system was previously modelled by Carter and coworkers and is an excellent sanity check for embedding theories.[16,18] The proton is transferred from a free fluoride to a micro-solvated one. The solvent molecules introduce asymmetry in the othwerwise symmetric potential energy curve of HFH^-.

Reaction coordinate is a distance between the free fluoride and the proton. Both fluorine atoms are fixed at the distance of 3.4 Å, whereas the proton is moved along the straight line connecting them. Each structure has been obtained by fixing the three atoms and performing constraint optimization at the MP2 level with 6-311+G** basis[35,36] using ORCA.[37]

The embedding energy calculations were performed with CP2K. Naturally, HFH^- is selected as a cluster, whereas four water molecules are treated as environment. PBE functional[38] was used to obtain the embedding potential, whereas MP2 served as a high-level method. GPW method was uitilized with Goedecker-Teter-Hutter pseudopotentials[39] obtained for PBE and Hartree-Fock, respectively, and a auxiliary plane-wave basis cutoff of 500 Ry. Correlation-consistent Gaussian basis for the of the triple-zeta quality[40] was used for the valence electrons together with the corresponding resolution-of-identity basis for the MP2 part. The cubic cell with a dimension of 30 Å was used together with a non-periodic

Poisson solver. SCF convergence criterion was set to 10^{-6} a.u. for both PBE and HF part of the MP2 calculations.

We were able to converge the embedding potential to 5×10^{-4} in the value of the maximum absolute value of the gradient, and to 5×10^{-3} in its Frobenius norm. Atoms contributing less than 5% to the sum of the gross atomic contributions were excluded by the potential reduction procedure.

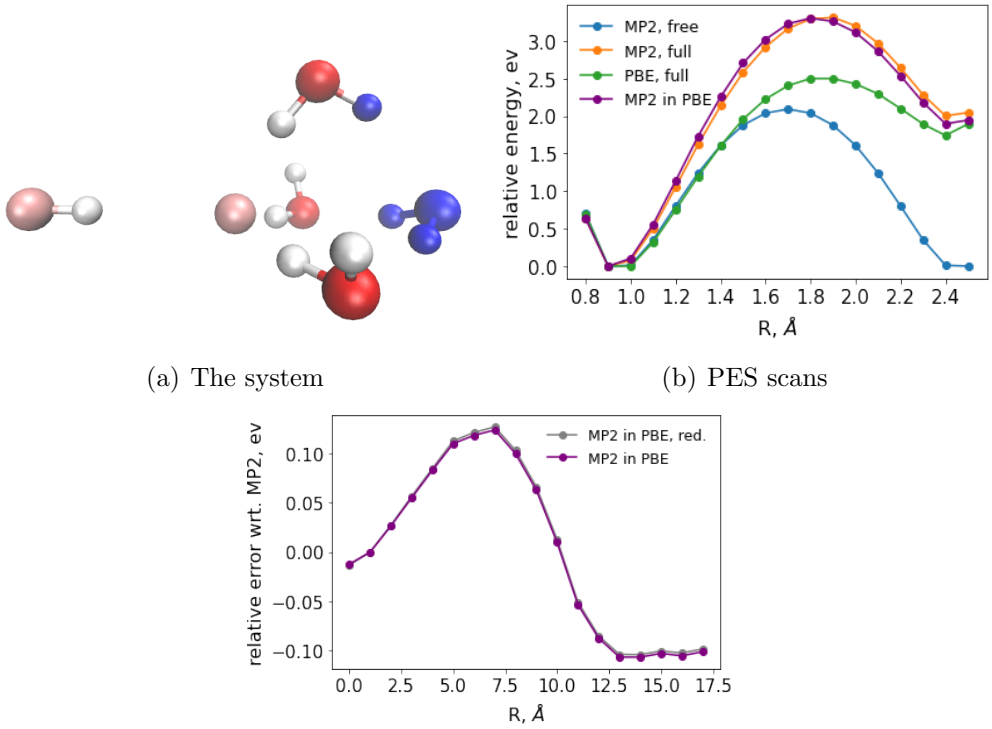

(a) The system

(b) PES scans

(c) Embedding errors

Figure 2: Application of the algorithm to a proton transfer reaction in the $(HFH^-)(H_2O)_4$ cluster. The proton (white) moves between the fixed fluorine atoms (pink). Atoms removed at potential reduction for most of the points are colored in blue. Methods used to generate potential energy curves are shown in legends. "red." stands for embedding with the reduced potential. Potential energy curves for embedded calculations with full and reduced potential are indistinguishable in the central panel.

As seen in Figure 2(b) the PES scan of the free cluster, FHF^-, is symmetric by construction, whereas with the solvent molecules added the proton prefers to stay with a "free" fluoride. The relative energy difference between the two mimina are very close for both MP2 and PBE, although PBE predicts a much lower barrier. Embedded MP2@PBE curves closely

follow the full MP2 curve, the errors increasing towards the transition state and the product (see Figure 2(c)) reaching ca. 0.1 eV (2.3 kcal/mol), *i. e.* the edge of chemical accuracy. The error curve looks remarkably similar to the curve generated with the Wu-Yang method in work,[16] despite the different computational set-up.

The potential reduction procedure performs excellently. Indeed, the difference between the embedded calculations with full and reduced potentials are negligible (see Figure 2(c)) and not seen in the scale of Figure 2(b), showing the PES scans. Noticeably, the reduced MP2@PBE curve remains smooth despite the fact that different number of atoms (9 to 11) have been included in the remaining reduced potential.

4.2 Realistic system: ionization of aqueous phenol

4.2.1 System preparation

We compute the rigid PES scan of proton transfer from the hydroxy-group of phenol to the adjacent water, starting from an equilibrated structure. Although this is a somewhat artificial process, it is instructive for method testing. Moreover, it can be brought in contact with the experimental reality by computing the transition free energy with DFT followed by introducing corrections for many-body correlation (with embedding methods or not) computed for selected snapshots using free-energy perturbation.[41]

The system contains one phenol molecule and 68 water molecules, corresponding to the solubility limit at ambient conditions. The cubic periodic simulation cell has a dimension of 12.97 Å, which corresponds to the experimental density of the concentrated phenol solution. The system has been equilibrated for 5 ps at 300 K in a NVT ensemble using the colored-noise Langevin thermostat.[42] For equilibration, we have used the PBE functional with empirical rVV10[43] dispersion corrections and TZV2P[44] basis sets with the corresponding GTH potentials. The auxiliary plane wave basis energy cutoff was 500 Ry.

4.2.2 Accuracy of embedding

For the embedding calculations we switched to the all-electron GAPW formalism with the standard quantum chemistry basis, 6-311G**,[35] the functional and plane wave cutoff being the same. Phenol molecule with one water molecule solvated the hydroxy-group is defined as cluster, whereas the rest of thesolvent served as environment as shown in Figure 3(a). We were able to converge the embedding potential to 1.0×10^{-3} in the value of the maximum absolute value of the gradient, and to 1.5×10^{-2} in its Frobenius norm. Atoms contributing less than 1.5% to the sum of the gross atomic contributions were excluded by the potential reduction procedure. This resulted in having 6 to 9 ghost atoms contributing to the reduced potential. As a higher-level method, the exact exchange (EXX) and RPA, EXX/RPA,[45] (later referred to simply as RPA) was used in its RI-variant[46] with the def2-SVP-RIFIT auxiliary basis set.[47]

The PES scan of proton transfer is shown in Figure 3(b). As in the previous example, the effect of solvent is huge, reducing the barrier almost by a factor of two (compare RPA, free and RPA, full curves in Figure 3(b)), whereas the effect of many-body correlation is moderate (PBE vs. various RPA curves). Embedded RPA curves reasonably accurately reproduce the full RPA one, errors not exceeding 0.1 eV (see Figure 3(c)). Although these errors are generally smaller than those in the $(HFH^-)(H_2O)_4$ cluster, they are more apparent in the case of phenol ionization as the energy scale and many-body correlation energies are smaller. Importantly, the Mulliken potential reduction leads to varying errors for different points. This is caused by varying number of ghost atoms automatically selected based on voluntaristically chosen threshold. The greatest deviations between the full and reduced embedded calculations are observed for the points between 0.15 and 0.35 Å, where only 6 ghost atoms were left. At the same time this error still does not exceed 0.1 eV as compared to the reference full RPA calculation and the deviation from the full embedded calculation is smaller. This problem is resolved by fixing the number of the ghost atoms to this found for the first point (here, 8). Then the reduced embedding curve closely follows the full

embedding curve with the maximum deviation of ca. 0.01 eV as shown in Fig. 3(b) and 3(c).

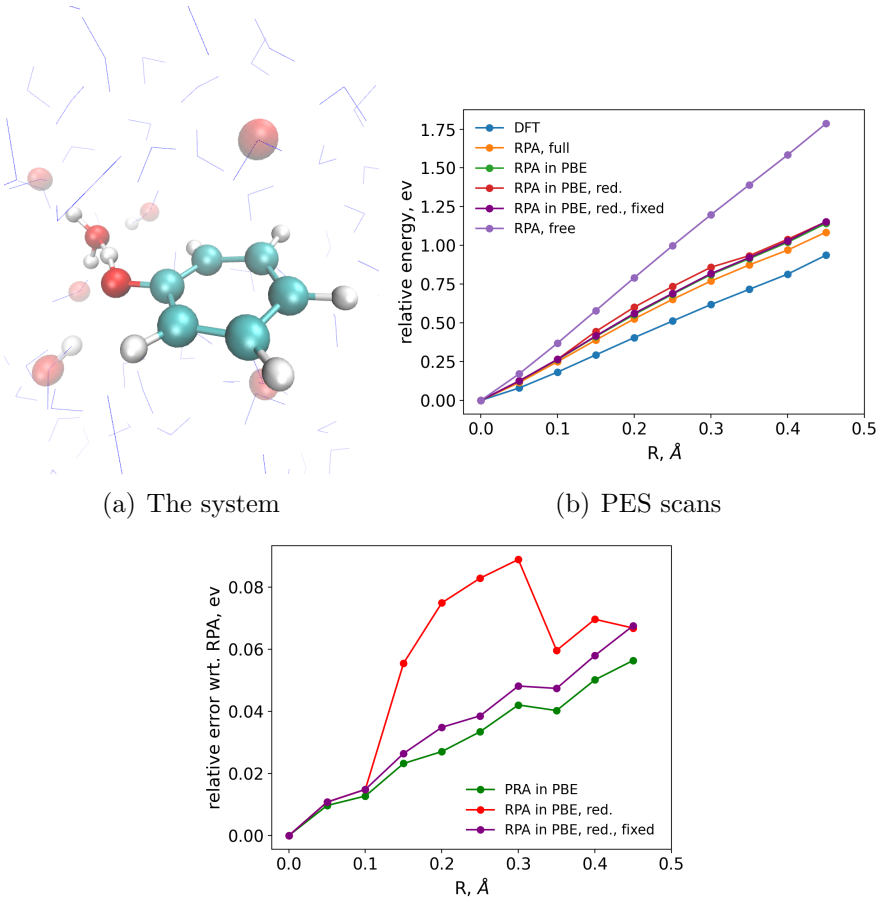

(a) The system

(b) PES scans

(c) Embedding errors

Figure 3: Application of the algorithm ionization of phenol in water. The proton moves between the the hydroxy-group of the phenol and the adjacent water molecule: phenol and this water molecule form the cluster. Ghost atoms included after the potential reduction colored and transparent. Atoms removed at potential reduction are shown as lines and colored in blue. Methods used to generate potential energy curves are shown in legends. "red." stands for embedding with the reduced potential. "fixed" stands for reduced embedding of RPA in PBE with the fixed number of ghost atoms to be included in the reduced potential.

4.2.3 Computational performance analysis

Let us now discuss computational performance of the embedding schemes. Some important timings are summarized in Table 1. The most expensive part of the Wu-Yang functional optimization is the exchange-like two-index integral contraction (denoted as opt. step in

Table 1), performed twice per optimization step as discussed above. The SCF on both subsystems takes similar amount of time at the first step. As the optimization progresses, the ASAP guess[48] reduces this effort dramatically as SCF converges within less than 5 cycles already before the tenth step (see Figure 4). The RI approximation for the four-center overlap integrals performs worse and is thus not recommended. Although it requires less memory, the conventional evaluation is not particularly memory-demanding either. The latter required only 6 GB of RAM with the Schwarz integral screening[29] threshold set to $10^{-}7$ a.u., whereas the exact exchange calculation needed for EXX/RPA needed 226 GB with the Schwarz screening threshold of $10 - 9$ a.u. Such a loose threshold for the overlap integrals naturally does not lead to considerable errors, which is not the case for the exact exchange integrals.

Another observation is that the cost of the embedded RPA calculation using the full basis set and potential costs almost as much as the full RPA calculation, which is to be expected, since the basis set size defines the size of the virtual space. On the other hand, the embedded RPA calculation with the reduced basis and potential costs only slighter more than the calculation on the free cluster, which highlights the critical importance of potential reduction.

At the same time, keeping in mind that it takes ca. 100 steps to obtain the embedding potential starting from scratch, we can see that the total price of the embedded calculation is compatible to this of the full embedding calculation. Here, a few note must be made. First, using converged matrix embedding potential from the adjacent point on the PES one may dramatically accelerate the convergence of the Wu-Yang functional optimization. Second, the full RPA calculation using CP2K for the aqueous phenol needs at least 32 Cray XC50 nodes (384 cores), i.e. HPC resources, whereas all calculations required for the embedding can be done on 6 nodes (72 cores) or on a typical local workstation. Third, the embedding potential is transferable and can thus be applied to any CW method used for the embedded cluster. In addition, having a converged matrix potential one may adjust the Mulliken

reduction criterion to obtain various reduced potentials, each practically requiring one optimization step (one exchange-like build) using the restart procedure. Most importantly, most CW methods scale steeper than the exchange-like build, also having a higher prefactor (with the exception of local-correlated methods). The RPA implementation used here scales as $\mathcal{O}(N^4 logN)$ (although it can scale cubically for very large systems[49,50]). Canonical coupled-cluster methods scale at least as $\mathcal{O}(N^6)$, multi-reference methods scale exponentially,[51] with the exception of locally correlated techniques.[52] Importantly, only a few of the are implemented for the condensed-phase.[53,54] On the other hand, the exchange-like build scales at most $\mathcal{O}(N^2)$ with the system size and at most as $\mathcal{O}(N^4)$ with the basis size,[27,29,51] i.e. like hybrid DFT although with a much smaller prefactor. Indeed, the Fock-build for the aqueous phenol takes 50 node-minutes as compared to 5 node-minutes in case of the exchange-like build using the four-center overlap integrals. Thus, with increasing system size, basis set and the complexity of CW the current matrix embedding scheme will become more and more economic as compared to the full CW calculations, should those be possible at all.

Finally, a note must be made on the differences between the grid-based embedding and the matrix-based embedding as proposed here. The former adds practically no additional cost to this of local DFT, let alone it does not change the scaling. The cost of matrix-based embedding is paid for smooth transition between the condensed-phase DFT and molecular implementations of the CW theories both in terms of potential representation and uniform treatment of pseudopotential and all-electron formalisms. Another price-increasing factor is the inevitable presence of the ghost atoms even after the potential reduction, although this is also recommended for the potentials on the grid.

Table 1: CPU wall times for the calculations of proton transfer in aqueous phenol. For potential optimization step (opt. step) two numbers are given separated by "/": conventional four-center integral evaluations and the one with RI-approximation; the number in parenthesis is the time for DFT calculations of the cluster and the environment after the first step. All simulations have been performed on the Piz Daint supercomuter of the Swiss National Supercomputer Centre using Cray XC50 compute nodes, consisting of 12 CPUs and one GPU.

Calculation	RPA, cluster	emb. RPA, red.	emb. RPA, full	full RPA	Opt. step/ RI
CPU time, node-min.	3.5	7	2895	2950	36/90 (6)
Compute nodes	6	6	32	32	6

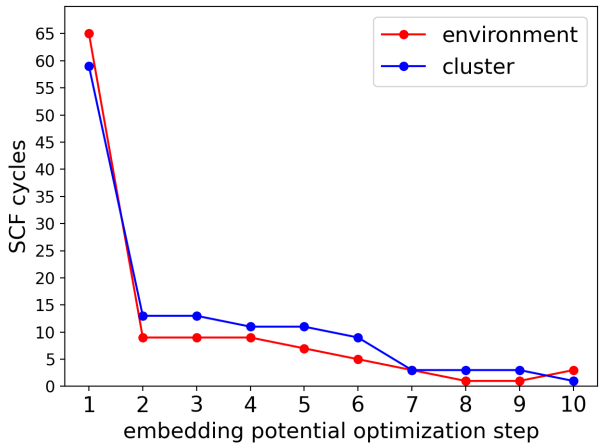

Figure 4: Number of cycles needed to converge the SCF of the subsystems in course of embedding potential optimization (maximization of the Wu-Yang functional).

5 Conclusions

In this work, embedding potential representation in finite basis using AO products has been introduced in the context of DFET, although it can be utilized for other embedding schemes. The formalism allows to treat both all-electron and pseudopotential calculations in a uniform fashion and transfer the embedding potential expressed in a compact matrix form between condensed-phase and molecular software based using Gaussian (or any other AO) basis sets. In addition, a simple semi-black-box procedure for basis set and embedding potential reduction critical for computational performance has been proposed. The formalism has been implemented in the CP2K program within GPW (pseudopotential calculations) and GAPW (pseudopotential and all-electron calculations) approaches and tested for proton transfer reactions in a cluster and a solution. Relative energies of the embedded calculations typically deviate from the reference MP2 and RPA within the range of 0.1 eV.

The algorithm can be applied to large systems, its computational bottleneck being the evaluation of the four-center exchange integrals and their two-index contraction, similar to exact-exchange Fock-build. Therefore, the algorithm scales as hybrid DFT ($\mathcal{O}(N^2)$ with the system size and as $\mathcal{O}(N^4)$ with the basis set size) with a significantly lower prefactor due to the simplicity of overlap integrals evaluation and their sparsity as compared with the exchange integrals.

Evaluated with the methods available in CP2K the implementation can now be applied to high-level correlated methods implemented in molecular software packages.

Acknowledgement

This work has been supported by the SNSF in the form of Ambizione grant No. PZ00P2_174227. Calculations have been performed at the Swiss National Supercomputing Centre (CSCS) using the resources under Project ID uzh1.

The author thanks Prof. J. Hutter and Dr. P. Seewald (both from University of Zurich)

for advice and fruitful discussions.

Supporting Information Available

The CP2K input files for matrix-based DFET calculations on the cluster system with the corresponding coordinates are available in the Supporting Information.

References

(1) Wesolowski, T. A.; Shedge, S.; Zhou, X. Frozen-Density Embedding Strategy for Multilevel Simulations of Electronic Structure. *Chemical Reviews* **2015**, *115*, 5891–5928, PMID: 25923542.

(2) Wesolowski, T. A.; Warshel, A. Frozen density functional approach for ab initio calculations of solvated molecules. *The Journal of Physical Chemistry* **1993**, *97*, 8050–8053.

(3) Sun, Q.; Chan, G. K.-L. Quantum Embedding Theories. *Accounts of Chemical Research* **2016**, *49*, 2705–2712, PMID: 27993005.

(4) Huang, C.; Pavone, M.; Carter, E. A. Quantum mechanical embedding theory based on a unique embedding potential. *The Journal of Chemical Physics* **2011**, *134*, 154110.

(5) Yu, K.; Carter, E. A. Extending density functional embedding theory for covalently bonded systems. *Proceedings of the National Academy of Sciences* **2017**, *114*, E10861–E10870.

(6) Knizia, G.; Chan, G. K.-L. Density Matrix Embedding: A Simple Alternative to Dynamical Mean-Field Theory. *Phys. Rev. Lett.* **2012**, *109*, 186404.

(7) Lan, T. N.; Kananenka, A. A.; Zgid, D. Communication: Towards ab initio self-energy embedding theory in quantum chemistry. *The Journal of Chemical Physics* **2015**, *143*, 241102.

(8) Fornace, M. E.; Lee, J.; Miyamoto, K.; Manby, F. R.; Miller, T. F. Embedded Mean-Field Theory. *Journal of Chemical Theory and Computation* **2015**, *11*, 568–580, PMID: 26580914.

(9) Ye, H.-Z.; Ricke, N. D.; Tran, H. K.; Van Voorhis, T. Bootstrap Embedding for Molecules. *Journal of Chemical Theory and Computation* **2019**, *15*, 4497–4506, PMID: 31343878.

(10) Yu, K.; Libisch, F.; Carter, E. A. Implementation of density functional embedding theory within the projector-augmented-wave method and applications to semiconductor defect states. *The Journal of Chemical Physics* **2015**, *143*, 102806.

(11) Zhao, Q.; Zhang, X.; Martirez, J. M. P.; Carter, E. A. Benchmarking an Embedded Adaptive Sampling Configuration Interaction Method for Surface Reactions: H2 Desorption from and CH4 Dissociation on Cu(111). *Journal of Chemical Theory and Computation* **2020**, *16*, 7078–7088, PMID: 33079552.

(12) Huang, C.; Carter, E. A. Potential-functional embedding theory for molecules and materials. *The Journal of Chemical Physics* **2011**, *135*, 194104.

(13) Yang, W.; Wu, Q. Direct Method for Optimized Effective Potentials in Density-Functional Theory. *Phys. Rev. Lett.* **2002**, *89*, 143002.

(14) Chung, L. W.; Sameera, W. M. C.; Ramozzi, R.; Page, A. J.; Hatanaka, M.; Petrova, G. P.; Harris, T. V.; Li, X.; Ke, Z.; Liu, F.; Li, H.-B.; Ding, L.; Morokuma, K. The ONIOM Method and Its Applications. *Chemical Reviews* **2015**, *115*, 5678–5796, PMID: 25853797.

(15) Schnieders, D.; Neugebauer, J. Accurate embedding through potential reconstruction: A comparison of different strategies. *The Journal of Chemical Physics* **2018**, *149*, 054103.

(16) Zhang, X.; Carter, E. A. Kohn-Sham potentials from electron densities using a matrix representation within finite atomic orbital basis sets. *The Journal of Chemical Physics* **2018**, *148*, 034105.

(17) Kollmar, C.; Neese, F. The static response function in Kohn-Sham theory: An appropriate basis for its matrix representation in case of finite AO basis sets. *The Journal of Chemical Physics* **2014**, *141*, 134106.

(18) Zhang, X.; Carter, E. A. Subspace Density Matrix Functional Embedding Theory: Theory, Implementation, and Applications to Molecular Systems. *Journal of Chemical Theory and Computation* **2019**, *15*, 949–960.

(19) Mulliken, R. S. Electronic Population Analysis on LCAO–MO Molecular Wave Functions. I. *The Journal of Chemical Physics* **1955**, *23*, 1833–1840.

(20) Kühne, T. D.; Iannuzzi, M.; Del Ben, M.; Rybkin, V. V.; Seewald, P.; Stein, F.; Laino, T.; Khaliullin, R. Z.; Schütt, O.; Schiffmann, F.; Golze, D.; Wilhelm, J.; Chulkov, S.; Bani-Hashemian, M. H.; Weber, V.; Borštnik, U.; Taillefumier, M.; Jakobovits, A. S.; Lazzaro, A.; Pabst, H.; Müller, T.; Schade, R.; Guidon, M.; Andermatt, S.; Holmberg, N.; Schenter, G. K.; Hehn, A.; Bussy, A.; Belleflamme, F.; Tabacchi, G.; Glöß, A.; Lass, M.; Bethune, I.; Mundy, C. J.; Plessl, C.; Watkins, M.; VandeVondele, J.; Krack, M.; Hutter, J. CP2K: An electronic structure and molecular dynamics software package - Quickstep: Efficient and accurate electronic structure calculations. *The Journal of Chemical Physics* **2020**, *152*, 194103.

(21) The code can be obtained from https://github.com/rybkinjr/cp2k/tree/mat_embed_new. Last accessed 28.12.2020.

(22) Lippert, B. G.; Hutter, J.; Parrinello, M. A hybrid Gaussian and plane wave density functional scheme. *Molecular Physics* **1997**, *92*, 477–488.

(23) Lippert, G.; Hutter, J.; Parrinello, M. The Gaussian and augmented-plane-wave density functional method for ab initio molecular dynamics simulations. *Theoretical Chemistry Accounts* **1999**, *103*, 124–140.

(24) Blöchl, P. E. Projector augmented-wave method. *Phys. Rev. B* **1994**, *50*, 17953–17979.

(25) Obara, S.; Saika, A. Efficient recursive computation of molecular integrals over Cartesian Gaussian functions. *The Journal of Chemical Physics* **1986**, *84*, 3963–3974.

(26) Valeev, E. F. Libint: A library for the evaluation of molecular integrals of many-body operators over Gaussian functions. http://libint.valeyev.net/, 2020; version 2.7.0-beta.6.

(27) Guidon, M.; Schiffmann, F.; Hutter, J.; VandeVondele, J. Ab initio molecular dynamics using hybrid density functionals. *The Journal of Chemical Physics* **2008**, *128*, 214104.

(28) Vahtras, O.; Almlöf, J.; Feyereisen, M. Integral approximations for LCAO-SCF calculations. *Chemical Physics Letters* **1993**, *213*, 514 – 518.

(29) Häser, M.; Ahlrichs, R. Improvements on the direct SCF method. *Journal of Computational Chemistry* **1989**, *10*, 104–111.

(30) Borstnik, U.; VandeVondele, J.; Weber, V.; Hutter, J. Sparse Matrix Multiplication: The Distributed Block-Compressed Sparse Row Library. *Parallel Computing* **2014**, *40*.

(31) Group, T. C. D. DBCSR: Distributed Block Compressed Sparse Row matrix library. 2020; `https://github.com/cp2k/dbcsr`.

(32) Fletcher, R. *Practical Methods of Optimization*, 2nd ed.; John Wiley & Sons: New York, NY, USA, 1987.

(33) Møller, C.; Plesset, M. S. Note on an Approximation Treatment for Many-Electron Systems. *Phys. Rev.* **1934**, *46*, 618–622.

(34) Eshuis, H.; Bates, J. E.; Furche, F. Electron correlation methods based on the random phase approximation. *Theoretical Chemistry Accounts* **2012**, *131*, 1084.

(35) Krishnan, R.; Binkley, J. S.; Seeger, R.; Pople, J. A. Self-consistent molecular orbital methods. XX. A basis set for correlated wave functions. *The Journal of Chemical Physics* **1980**, *72*, 650–654.

(36) Clark, T.; Chandrasekhar, J.; Spitznagel, G. W.; Schleyer, P. V. R. Efficient diffuse function-augmented basis sets for anion calculations. III. The 3-21+G basis set for first-row elements, Li–F. *Journal of Computational Chemistry* **1983**, *4*, 294–301.

(37) Neese, F. Software update: the ORCA program system, version 4.0. *WIREs Computational Molecular Science* **2018**, *8*, e1327.

(38) Perdew, J. P.; Burke, K.; Ernzerhof, M. Generalized Gradient Approximation Made Simple. *Phys. Rev. Lett.* **1996**, *77*, 3865–3868.

(39) Goedecker, S.; Teter, M.; Hutter, J. Separable dual-space Gaussian pseudopotentials. *Phys. Rev. B* **1996**, *54*, 1703–1710.

(40) Del Ben, M.; Hutter, J.; VandeVondele, J. Electron Correlation in the Condensed Phase from a Resolution of Identity Approach Based on the Gaussian and Plane Waves Scheme. *Journal of Chemical Theory and Computation* **2013**, *9*, 2654–2671.

(41) Chehaibou, B.; Badawi, M.; Bučko, T.; Bazhirov, T.; Rocca, D. Computing RPA Adsorption Enthalpies by Machine Learning Thermodynamic Perturbation Theory. *Journal of Chemical Theory and Computation* **2019**, *15*, 6333–6342, PMID: 31614086.

(42) Ceriotti, M.; Bussi, G.; Parrinello, M. Colored-Noise Thermostats à la Carte. *Journal of Chemical Theory and Computation* **2010**, *6*, 1170–1180.

(43) Sabatini, R.; Gorni, T.; de Gironcoli, S. Nonlocal van der Waals density functional made simple and efficient. *Phys. Rev. B* **2013**, *87*, 041108.

(44) VandeVondele, J.; Hutter, J. Gaussian basis sets for accurate calculations on molecular systems in gas and condensed phases. *The Journal of Chemical Physics* **2007**, *127*, 114105.

(45) Fuchs, M.; Gonze, X. Accurate density functionals: Approaches using the adiabatic-connection fluctuation-dissipation theorem. *Phys. Rev. B* **2002**, *65*, 235109.

(46) Eshuis, H.; Yarkony, J.; Furche, F. Fast computation of molecular random phase approximation correlation energies using resolution of the identity and imaginary frequency integration. *The Journal of Chemical Physics* **2010**, *132*, 234114.

(47) Weigend, F.; Häser, M.; Patzelt, H.; Ahlrichs, R. RI-MP2: optimized auxiliary basis sets and demonstration of efficiency. *Chemical Physics Letters* **1998**, *294*, 143 – 152.

(48) Kolafa, J. Time-reversible always stable predictor–corrector method for molecular dynamics of polarizable molecules. *Journal of Computational Chemistry* **2004**, *25*, 335–342.

(49) Kaltak, M.; Klimeš, J.; Kresse, G. Low Scaling Algorithms for the Random Phase Approximation: Imaginary Time and Laplace Transformations. *Journal of Chemical Theory and Computation* **2014**, *10*, 2498–2507, PMID: 26580770.

(50) Wilhelm, J.; Seewald, P.; Del Ben, M.; Hutter, J. Large-Scale Cubic-Scaling Random Phase Approximation Correlation Energy Calculations Using a Gaussian Basis. *Journal of Chemical Theory and Computation* **2016**, *12*, 5851–5859, PMID: 27779863.

(51) Helgaker, T.; Jørgensen, P.; Olsen, J. *Molecular Electronic Structure Theory*; John Wiley & Sons, LTD: Chichester, 2000.

(52) Usvyat, D.; Maschio, L.; Schütz, M. Periodic and fragment models based on the local correlation approach. *WIREs Computational Molecular Science* **2018**, *8*, e1357.

(53) Zhang, I. Y.; Grüneis, A. Coupled Cluster Theory in Materials Science. *Frontiers in Materials* **2019**, *6*, 123.

(54) Rybkin, V. V. Sampling Potential Energy Surfaces in the Condensed Phase with Many-Body Electronic Structure Methods. *Chemistry – A European Journal* **2020**, *26*, 362–368.

Graphical TOC Entry